1-1-2013

Mitigation of rooftop solar PV impacts and evening peak support by managing available capacity of distributed energy storage systems

Md Jan-E- Alam
University of Wollongong, mjea982@uowmail.edu.au

Kashem Muttaqi
University of Wollongong, kashem@uow.edu.au

Darmawan Soetanto
University of Wollongong, soetanto@uow.edu.au

Mitigation of rooftop solar PV impacts and evening peak support by managing available capacity of distributed energy storage systems

Abstract

A high penetration of rooftop solar photovoltaic (PV) resources into low-voltage (LV) distribution networks creates reverse power-flow and voltage-rise problems. This generally occurs when the generation from PV resources substantially exceeds the load demand during high insolation period. This paper has investigated the solar PV impacts and developed a mitigation strategy by an effective use of distributed energy storage systems integrated with solar PV units in LV networks. The storage is used to consume surplus solar PV power locally during PV peak, and the stored energy is utilized in the evening for the peak-load support. A charging/discharging control strategy is developed taking into account the current state of charge (SoC) of the storage and the intended length of charging/discharging period to effectively utilize the available capacity of the storage. The proposed strategy can also mitigate the impact of sudden changes in PV output, due to unstable weather conditions, by putting the storage into a short-term discharge mode. The charging rate is adjusted dynamically to recover the charge drained during the short-term discharge to ensure that the level of SoC is as close to the desired SoC as possible. A comprehensive battery model is used to capture the realistic behavior of the distributed energy storage units in a distribution feeder. The proposed PV impact mitigation strategy is tested on a practical distribution network in Australia and validated through simulations. 2013 IEEE.

Keywords

energy, distributed, capacity, mitigation, available, managing, support, peak, rooftop, evening, solar, impacts, storage, systems, pv

Disciplines

Engineering | Science and Technology Studies

Publication Details

Mitigation of Rooftop Solar PV Impacts and Evening Peak Support by Managing Available Capacity of Distributed Energy Storage Systems

M. J. E. Alam, *Student Member, IEEE*, K. M. Muttaqi, *Senior Member, IEEE* and D. Sutanto, *Senior Member, IEEE*

Abstract—**A high penetration of rooftop solar photovoltaic (PV) resources into low-voltage (LV) distribution networks creates reverse power-flow and voltage-rise problems. This generally occurs when the generation from PV resources substantially exceeds the load demand during high insolation period. This paper has investigated the solar PV impacts and developed a mitigation strategy by an effective use of distributed energy storage systems integrated with solar PV units in LV networks. The storage is used to consume surplus solar PV power locally during PV peak, and the stored energy is utilized in the evening for the peak-load support. A charging/discharging control strategy is developed taking into account the current state of charge (SoC) of the storage and the intended length of charging/discharging period to effectively utilize the available capacity of the storage. The proposed strategy can also mitigate the impact of sudden changes in PV output, due to unstable weather conditions, by putting the storage into a short-term discharge mode. The charging rate is adjusted dynamically to recover the charge drained during the short-term discharge to ensure that the level of SoC is as close to the desired SoC as possible. A comprehensive battery model is used to capture the realistic behavior of the distributed energy storage units in a distribution feeder. The proposed PV impact mitigation strategy is tested on a practical distribution network in Australia and validated through simulations.**

Index Terms—**Rooftop solar photovoltaic, Energy storage, Reverse power flow, Voltage-rise, Charging/discharging strategy.**

I. INTRODUCTION

SOLAR photovoltaic (PV) resources are the most commonly observed form of distributed generation (DG) at the residential customer premises in low voltage (LV) distribution networks. Depending on their capacity, the rooftop solar PV units serve part of the loads locally that reduces the stress on the distribution feeder and improve system performance by reducing feeder loss and releasing system capacity. However, a high penetration level of PV resources can impose several challenges for distribution network operators, such as, reverse power-flow and voltage-rise problems at LV networks [1-4].

If the PV generation is greater than the local demand at the point of common coupling (PCC), the excess power from PV inverters may produce reverse power flow in the feeder that would create voltage-rise [2, 4]. With a high penetration of rooftop PV resources at LV level, there is a possibility of the upper voltage limit violation. Solutions are required to reduce the overvoltage problem caused by the rooftop solar PV so that the penetration level can be increased while preserving a compliance with the system operation limits.

Active power curtailment [5] and reactive power consumption [6] have been proposed for voltage-rise mitigation. Active power curtailment may not be an economically attractive solution, while reactive power consumption may create additional loss in the feeder due to higher current flow [7]. Authors in [8] have proposed a reactive power based voltage control technique to mitigate the voltage-rise and also discussed the limitations of their technique. Authors in [9] have proposed a control strategy for a coordinated operation of the energy storage systems and On-Load Tap Changers (OLTCs) for voltage-rise mitigation, that reduces tap changer operation stress and feeder power loss. However, an aggregate model of the secondary LV circuits was used and the details of storage charging and discharging profiles were not presented, as the focus of the paper was mainly on control coordination. The application of storage devices integrated with residential PV systems was proposed in [10] to store the surplus power from the PV array during noon time and hence reducing the energy loss associated with the excess power from the solar PV. This operation can also reduce the reverse power flow and voltage-rise problems during peak PV generation by injecting less power to the grid and storing the excess energy in the battery storage. Stored energy could be used to support the evening peak load by serving the local loads and hence reducing the stress on the grid. An investigation of voltage-rise mitigation is presented in [11] using detailed models of solar PV and battery storage devices. However, a constant-rate charging/discharging strategy was used in [11] that makes the storage device to consume or generate a constant power over the charging or discharging period, irrespective of the PV generation and the load demand variations.

In this paper, a new charging/discharging strategy is proposed for storage devices integrated with rooftop PV systems that can better match the PV generation and load

profile. The proposed strategy is more advantageous for PV impact mitigation and evening load support compared to the traditional constant charging/discharging strategy. To wisely use the limited capacity of the storage device, while operating it according to the proposed strategy, a methodology is developed to obtain the appropriate charging/discharging rates. The proposed charging/discharging strategy would also be able to mitigate sudden changes in PV output (due to unstable weather conditions, such as, cloud passing) by operating the storage in a short-term discharge mode. The proposed strategy can also track the deviation of the actual State of Charge (SoC) of the energy storage device with the expected level of SoC at any given time instant. If the deviation of the actual SoC is more than a specified level, an adjustment of the charging/discharging rate is performed to compensate for such a deviation. This will ensure a better utilization of the available storage capacity. The proposed control strategies are verified using an Australian distribution system where the LV secondary circuits are explicitly modeled using distributed household loads, rooftop solar PV arrays and distributed storage systems.

II. ANALYSIS OF PCC OPERATION UNDER PV PENETRATION

A simple feeder shown in Fig. 1(a) is used to illustrate the voltage-rise issues produced by the solar PV units in a distribution feeder. The PV panels and storage devices are connected to the PCCs through Power Conditioning Systems (PCS) that perform Maximum Power Point Tracking (MPPT), storage control and DC/AC conversion. Initially, the storage devices are considered to be absent. Without PV, a voltage drop would occur along the feeder, as shown in Fig. 1(b). With PV, if all the loads are locally served by the PV generations at each of the PCCs, the voltage profile would be nearly flat as in Fig. 1(c). However, if the PV generation exceeds the load demand, especially at the furthest end of the feeder, then the power will flow back from the feeder to the upstream network and this can cause the voltage to rise, as shown in Fig. 1(d).
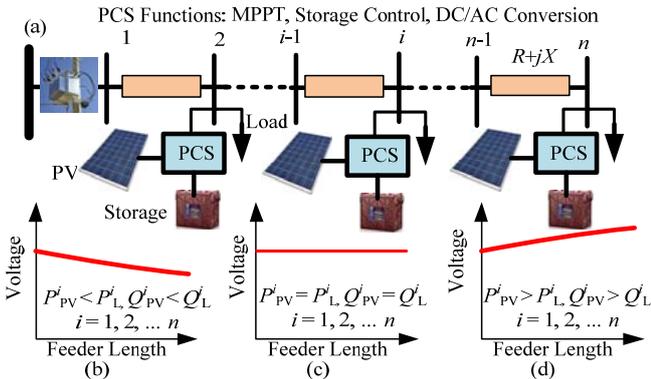

Fig. 1. Voltage profile along feeder with different PV generation. (a) single line diagram of feeder; (b) voltage drop (c) flat voltage profile (d) voltage-rise.

A four quadrant P-Q diagram shown in Fig. 2(a) is used to illustrate the PCC operation under PV penetration where the active power (P) and the reactive power (Q) of the PV inverter can be fully controlled. From the perspective of a power injection, the loads and the power injections from the solar PV are shown in the negative and positive P and Q axes, respectively. Hence, a PCC operating in the 1st quadrant behaves like a source, and in the 3rd quadrant behaves like a load. Therefore, a 1st quadrant operation of the PCC would normally cause a voltage-rise, and a 3rd quadrant operation would cause a voltage drop. However, a 2nd quadrant or a 4th quadrant operation would cause the PCC to be either a P-sink and Q-source, or a P-source and Q-sink, respectively. A 2nd quadrant operation may cause a voltage-rise with a net positive Q injection if the network is highly reactive, whereas, a 4th quadrant operation may cause a voltage-rise if the network is highly resistive.
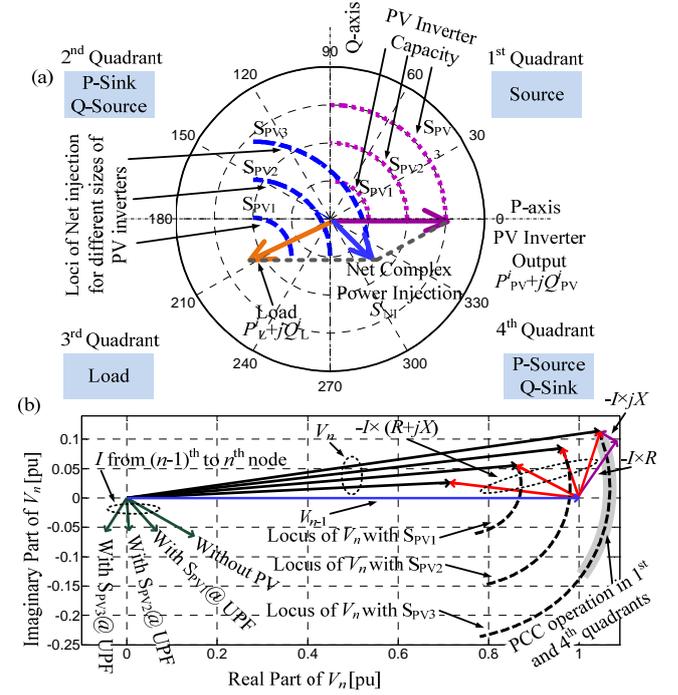

Fig. 2. Loci of net power injection and voltage. (a) Net power injection with different PV capacity; (b) Voltage for different amount of PV injection.

The net complex power injection at the i-th node, S^i_{NI}, can be expressed as,

$$S^i_{NI} = \left(P^i_{PV} - P^i_L\right) + j\left[\sqrt{\left(S^i_{PV}\right)^2 - \left(P^i_{PV}\right)^2} - Q^i_L\right] \quad (1a)$$

where, $P^i_{PV} + jQ^i_{PV}$ is the complex power generated by the PV inverter at the i-th node, S^i_{PV} is the PV inverter capacity, and $P^i_L + jQ^i_L$ is the load connected at this node. However, for a unity power factor (UPF) operation of the inverter where the reactive (Q) injection/absorption is *zero*, (1a) can be simplified as given in (1b).

$$S^i_{NI} = \left(P^i_{PV} - P^i_L\right) - jQ^i_L \quad (1b)$$

To investigate the effects of varying the outputs of the PV inverter on the PCC operation, the potential apparent capacities of PV inverter (S_{PV}) of 0.5, 1.0 and 1.5 times the load active power are considered, and denoted with S_{PV1}, S_{PV2}, and S_{PV3}, respectively, as shown using the dotted circular lines in the 1st quadrant. The active power output of the PV inverter in the P-axis is varied from the rated capacity to *zero* in the 1st quadrant of Fig. 2(a). The remaining capacity is used for reactive power injection. Considering a fixed load and the

variations of PV inverter output as stated for each of the inverter capacities, S_{PV1}, S_{PV2}, and S_{PV3}, the tips of the net power injection vectors obtained using (1a) are plotted as the loci of the net injections in Fig. 2(a). These loci represent the operating points of the PCC as the PV inverter output varies. For an inverter capacity S_{PV1}, less than the load active power, the PCC operation remains within the 2nd and 3rd quadrant for the entire range of the PV inverter output variations. For an inverter capacity S_{PV2}, equal to the load active power, the operating point of the PCC starts at the edge of the 3rd quadrant when the inverter active power output is at the rated value, and gradually shifts into the 2nd quadrant, as the inverter output is varied. For an inverter capacity S_{PV3}, higher than the load active power, the PCC operation traverses through the 4th, 1st and 2nd quadrant, but does not enter into the 3rd quadrant. This indicates that for such an inverter capacity, the PCC may behave either as a PQ-source, or a P-source Q-sink, or a P-sink Q-source, but it will not behave like a load.

Ideally, for a highly resistive distribution circuit, the reverse power flow and voltage-rise problem would exist while the operating point of the PCC is located in the 1st and the 4th quadrant. This can be illustrated using a 2-node segment of the feeder in Fig. 1(a), from the $(n-1)$-th to the n-th node. A load and a PV inverter are connected at the n-th node and the output of the inverter is varied according to the capacity curves in the 1st quadrant of Fig. 2(a). The line impedance $(R+jX)$ corresponds to a highly resistive distribution circuit and the load power factor used is similar to that of a low voltage residential feeder load. The voltages at the n-th node are obtained using a load flow analysis. The vector diagram of the voltages at these nodes is given by (2) and is shown in Fig. 2(b) using V_{n-1} as the reference vector.

$$V_n = V_{n-1} - [I \times (R + jX)] \qquad (2)$$

The tips of the voltage vector at the n-th node, V_n, are plotted in Fig. 2(b) for the variations in PV output for the three potential capacities of the PV inverter, S_{PV1}, S_{PV2}, and S_{PV3}, and indicated as the loci of the V_n. The voltage-rise is only observed for S_{PV3}, which is higher than the load active power and when the net P injection is positive. This is shown as the shaded region of the V_n locus for S_{PV3}. Therefore, a mechanism that can reduce the active power output of the solar PV inverter can help to mitigate the voltage-rise issue. This can be achieved by absorbing part of the solar PV inverter output in the storage device.

III. THE APPLICATION OF DISTRIBUTED ENERGY STORAGE FOR MITIGATION OF SOLAR PV IMPACTS

Storage devices will reduce the net active power injection so that the PCC operating point shifts towards the 2nd and 3rd quadrant where a voltage-rise would not be typically expected for a highly resistive distribution circuit. The shift of the net injection vector due to the addition of storage devices in the feeder of Fig. 1(a) is shown in Fig. 3(a) and the corresponding voltage vector at the n-th node is shown in Fig. 3(b). The addition of the storage device mitigates the voltage-rise by storing the surplus power from the solar PV in the storage

device. During the evening peak load period, the net injection vector would be shifted from the 3rd quadrant to the right towards the 4th quadrant, as shown in Fig. 4(a).
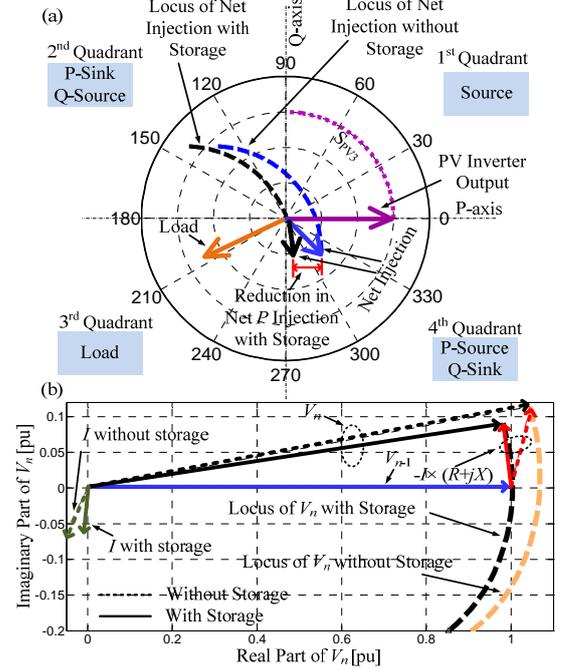
Fig. 3. A four quadrant net power injection diagram with storage. (a) Net injection in charging operation; (b) Voltage locus in charging operation.
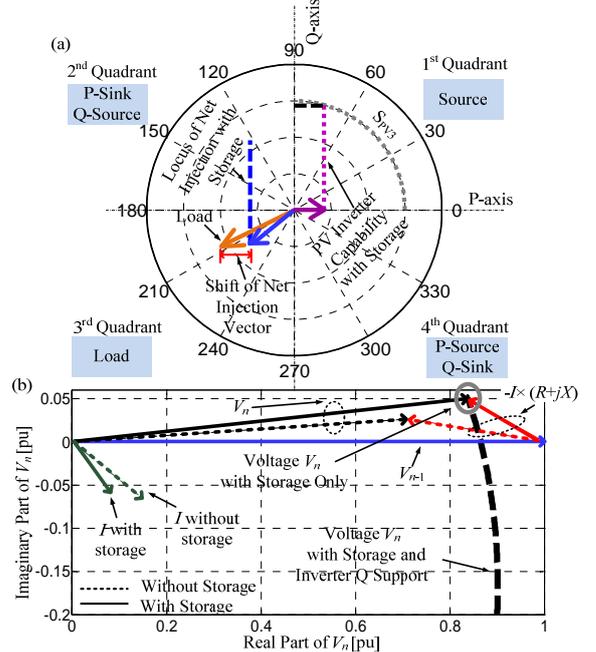
Fig. 4. Four quadrant net power injection diagram with storage: (a) Net injection in charging operation; (b) Voltage locus in discharge operation.

The corresponding voltage vector diagram is shown in Fig. 4(b) showing the voltage improvement that can be obtained with the storage device. If the remaining capacity of the inverter can be used for reactive power injection, as shown in the net injection locus of Fig. 4(a), a further improvement in voltage could be observed, as shown in the voltage locus of Fig. 4(b).

A. Modeling of Battery Storage Device for Rooftop Solar PV System

Rooftop PV installations at LV customer premises mainly consist of the solar PV modules that produce DC power from solar insolation, and a Power Conditioning System (PCS) that accomplishes multiple functions including maximum power point tracking, DC-AC conversion and filtering. For an integrated storage device coupled with the DC side of the rooftop PV system, as used in this paper, the PCS will also function as the charge/discharge controller. A detailed description of the rooftop PV system modeling is presented in the previous paper of the authors [11] and therefore is not included in this paper. More focus has been given on the modeling of storage devices and its charging/discharging strategies.

The modeling of the battery storage device involves obtaining the non-linear characteristics of the battery voltage as a function of the battery State of Charge (SoC) [12] at a given charging/discharging rate, as shown in Fig. 5 [13], for typical lead-acid batteries. In Fig. 5, C is the capacity of battery storage unit in Ampere-hour (Ah).
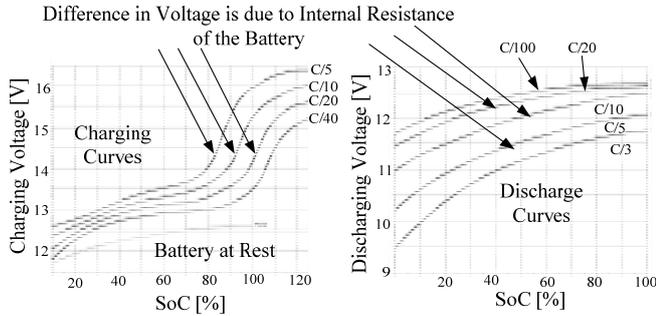

Fig. 5. Charge and discharge characteristic of a typical battery storage unit.

Fig. 5 shows that the battery voltage characteristics are different for the different charging/discharging rates due to the internal resistance of the battery [14]. The battery voltage varies throughout the whole range of SoC, as the internal resistance is a function of SoC [15]. When the battery is at rest, the voltage becomes lower [13]. The manufacturer supplied battery characteristic curves are segregated into exponential, nominal and end of nominal regions in [16], and a set of parameters is obtained to fit the characteristic curves containing the segregated regions. This model requires only three points to be taken from the manufacturer supplied curve. The model used in [16] uses the same characteristics for both charging and discharging operation. However, as shown in Fig. 5, the voltage value when charging, is different to that when discharging for a given SoC, because when the battery is discharged, the energy used to charge the battery is not fully recovered [17]. Furthermore, the internal resistance of the battery storage is different at charged and discharged states [18]. In this paper, separate charging/discharging curves and different internal resistances at charged and discharged states are considered to develop a more realistic battery model.

The battery voltage at a given charging/discharging rate can be expressed using (3) involving the battery capacity C_B, the present SoC, the battery internal resistances at charged state and at discharged state, R_{BC} and R_{BD}, the change in internal resistance for per unit change in SoC, ρ, and the battery current, I_B.

$$V_B = \begin{cases} V_{B0} + I_B(R_{BD} - \rho \times \text{SoC}), \text{ in charging operation} \\ V_{B0} - I_B(R_{BC} + \rho \times \text{SoC}), \text{ in discharge operation} \end{cases} \quad (3)$$

where, the no-load battery voltage, V_{B0} is given by [16],

$$V_{B0} = V_{BC} - K \times \frac{C_B}{C_B - \text{SoC}} + Ae^{-B \times \text{SoC}} \quad (4)$$

where, V_{BC} is the battery constant voltage; K is the polarization voltage; A is the exponential zone voltage; and B is the exponential zone time constant.

Methods for determining V_{B0}, K, A, and B are described in [16]. The model used in this paper requires first to obtain the set of parameters V_{B0}, K, A, and B for both charging and discharging curves at a given standard rate. The obtained parameters are then used in (3) and (4) to obtain the characteristic curves at the required charging and discharging rates.

The present SoC can be found from the previous SoC of the battery, the battery current, and the time interval between the previous and the present charging states as given in (5),

$$\text{SoC}(t + \Delta t) = \begin{cases} \text{SoC}(t) + I_B \Delta t, \text{ in charging operation} \\ \text{SoC}(t) - I_B \Delta t, \text{ in discharge operation} \end{cases} \quad (5)$$

B. Determination of the Maximum Charging Rate for Storage

Battery storage devices consume the surplus power from solar PV units during charging operation. This reduces the amount of active power injection into the grid. The injection of real power into the grid, P_{inj}, for a given level of load, PV output and battery storage unit can be obtained using (6).

$$P_{inj} = -P_L + \eta_{inv}(P_{PV} - \text{CR} \times V_B) \quad (6)$$

where, P_L is the active power of load, P_{PV} is the active power output of the PV module, η_{inv} is the PV inverter efficiency, CR is the battery charging rate, i.e., the battery current and V_B is the battery voltage.

A study was conducted to determine the amount of P_{inj} with a 1-kW load, which is a typical midday load of a residential household, and a 3-kW PV system. The values of P_{inj} at different charging rates are shown in Fig. 6 for a 12-V, 250-Ah battery.
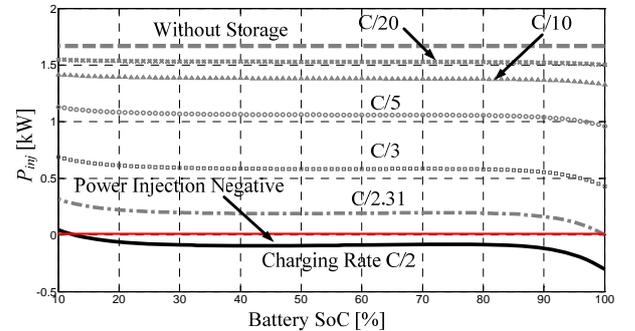

Fig. 6. The variation of power injection into grid at different charging rates.

The amount of grid injection decreases as the charging rate increases and this contributes to a mitigation of voltage-rise. However, beyond a certain level of charging rate, the battery power input will exceed the available surplus power from the

PV resulting in a negative PV power injection into the grid. Fig. 6 shows that a charging rate of C/2.31 will result in a negative P_{inj} at 100% SoC level of the battery, which is undesirable. The maximum allowable charging rate is the one at which the real power injection into the grid is *zero*, that is, all the surplus power is consumed by the storage during its charging operation. This rate could be obtained from (6) by putting *zero* for P_{inj}, as given in (7).

$$\text{CR}_{max} = \left| -\frac{(P_{L\min} - \eta_{inv} P_{PV\max})}{\eta_{inv} \times V_B^{\text{Full}}} \right| \quad (7)$$

In (7), $P_{L\min}$ is the minimum level of load within the PV generation period, $P_{PV\max}$ is the maximum amount of solar PV generation in the same period, and V_B^{Full} is the battery voltage at the 100% SoC. V_B^{Full} is a function of the charging rate and hence (7) is solved numerically to find CR_{max}.

C. A New Strategy for the Charging/Discharging of Storage Devices

In a clear sunny day, the PV output increases gradually as the day progresses, reaches its peak during midday, and gradually decreases after midday. The surplus power at the PCC would also follow a similar trend. Therefore, a charging strategy where the charging rate gradually increases with the progress of the day, reaches its peak level during midday, and gradually decreases after the midday, would be more effective for PV impact mitigation, compared to a traditional constant charging strategy. Similarly, a discharging strategy where the discharging rate gradually increases from the start of the evening period, reaches its peak level during the evening peak load, and gradually decreases with the decrease of evening load, would be more effective for peak load support compared to a constant discharging strategy.

Further, since the energy storage devices have limited capacity (Ah) or energy (kWh), it is important to use it wisely. Too fast charging of the energy storage, when there is reverse power flow, may cause the battery to be full too soon and therefore may result in unacceptable reverse power flow and a voltage-rise at an inconvenient time, for example at peak insolation period. But too slow charging of the storage device, when there is reverse power flow, may cause some of the capacity of the battery to be left unused.

A new charging/discharging strategy is proposed to better match the surplus PV generation/evening load profile. The methodology to obtain the appropriate charging/discharging rates to wisely use the limited storage capacity is described below using Fig. 7.

Fig. 7(a) shows the load and the PV output profile at a given PCC, where the PV output is higher than the load demand for a period of the day, T. During this period, a surplus power will be available at the PCC. According to the proposed strategy, the storage device will be charged over the period T. The charging rate will be increased from *zero* at the start of the period T, (when the storage SoC is at the maximum depth of discharge DoD_{max}) at a Slope of Charging Rate (SCR) defined in per-unit of time, until the SoC reaches a threshold level, ToS_1. This is shown in Fig. 7(b). From this point, the

storage will be charged at a constant saturated charging rate, CR_{Sat}. Once the SoC reaches the second threshold, ToS_2, less capacity of the storage is available and therefore the charging rate will be decreased using the same SCR, until the storage device attains the state of maximum charge, SoC_{max}, at the end of period T.
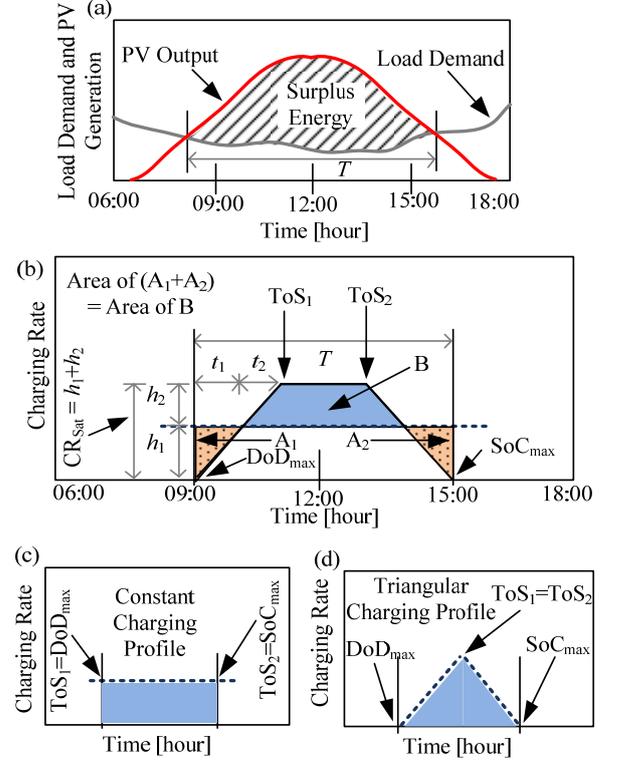

Fig. 7. Proposed charging/discharging strategy. (a) load and PV generation profile; (b) methodology to obtain charging/discharging rates; (c) a constant charging profile; (d) a triangular charging profile.

According to this strategy, the charging rate at the k-th time instant can be expressed as given in (8).

$$\text{CR}(k) = \begin{cases} \text{CR}(k-1) + \text{SCR}, \text{ if } \text{SoC}(k-1) \leq \text{ToS}_1 \\ \text{CR}_{\text{Sat}}, \text{ if } \text{ToS}_1 < \text{SoC}(k-1) < \text{ToS}_2 \\ \text{CR}(k-1) - \text{SCR}, \text{ if } \text{SoC}(k-1) \geq \text{ToS}_2 \\ 0, \text{ if } \text{SoC}(k-1) \geq \text{SoC}_{max} \end{cases} \quad (8)$$

To obtain the appropriate values of the parameters SCR and CR_{Sat} to be used in (8), the following facts are considered.

The amount of charge lost for not charging the battery at a constant charging rate over the entire charging period will have to be recovered in the overall charging period. Mathematically, this constraint can be expressed using the geometrical relationships in Fig. 7(b) as given below.

$$h_2^2 + (2h_1 - T \times \text{SCR}) \times h_2 + h_1^2 = 0 \quad (9)$$

where, h_1 is the constant charging rate that charges the battery in T amount of time, h_2 is the amount of increase in the constant charging rate to recover the charge lost for not using the constant charging rate over the whole charging period.

Again, the charge stored during the constant charging period is equal to the amount of charge between the first and second threshold of SoC, ToS_1 and ToS_2 respectively. This can be expressed using (10) below.

$$(h_1 + h_2) \times \left(T - \frac{2h_1}{\text{SCR}} - \frac{2h_2}{\text{SCR}}\right) - (\text{ToS}_2 - \text{ToS}_1) \times C = 0 \quad (10)$$

It is observed that in (9) and (10), h_2 and SCR are the only unknown parameters; h_1 is known from the battery capacity, and T is the period for which the battery is intended to be charged, which can be estimated from historical load and PV output profile as shown in Fig. 7(a), ToS_1 and ToS_2 are the choices to shape the charging rate profile. Therefore, h_2 and SCR can be obtained by solving (9) and (10) simultaneously using a numerical technique. By varying the difference between ToS_1 and ToS_2, different charging profiles can be obtained and the pattern of usage of the available storage capacity can be controlled. For example, if ToS_1 and ToS_2 are set to $\text{DoD}_{\max}$ and $\text{SoC}_{\max}$, respectively, a constant charging profile is obtained, as shown in Fig. 7(c). Again, if the difference between ToS_1 and ToS_2 is *zero*, then a triangular charging profile is obtained, as shown in Fig. 7(d).

A similar strategy will be followed for the discharge operation; however, in this case the discharge rate (DR) will be increased at a Slope of Discharge Rate (SDR) defined in per-unit of time, until the SoC drops to ToS_2 from the $\text{SoC}_{\max}$ level, and then the discharge will continue at a constant saturated discharge rate DR_{Sat}. When the SoC drops below ToS_1, the battery discharge rate is decreased at the same SDR until $\text{DoD}_{\max}$ is reached. At a given k-th instant, this can be expressed as,

$$\text{DR}(k) = \begin{cases} \text{DR}(k-1) + \text{SDR}, & \text{if } \text{SoC}(k-1) \geq \text{ToS}_2 \\ \text{DR}_{\text{Sat}}, & \text{if } \text{ToS}_2 > \text{SoC}(k-1) > \text{ToS}_1 \\ \text{DR}(k-1) - \text{SDR}, & \text{if } \text{SoC}(k-1) \leq \text{ToS}_1 \\ 0, & \text{if } \text{SoC}(k-1) \leq \text{DoD}_{\max} \end{cases} \quad (11)$$

The values of SDR and DR_{Sat} can be obtained from (9)-(10). In this case, T will be the intended period of discharge. This is the duration of the peak load support and will depend on the limited amount of the stored energy in the battery. To make an effective use of the available stored energy, it needs to be discharged in a period that includes the maximum evening peak, as shown in Fig. 8.
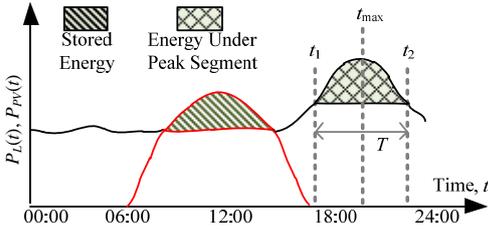

Fig. 8. Determination of evening peak support interval.

An estimate of the discharge period, T, can be obtained initially using the historical load curves of the specific household where the storage device is to be installed. If the available energy is fully discharged during the evening peak, the following expression will hold true.

$$\eta_B \times (\text{SoC}_{\max} - \text{DoD}_{\max}) \times V_B - \int_{t_1}^{t_2} P_L(t)dt = 0 \quad (12)$$

where, $(t_2 - t_1) = T$, as shown in Fig. 8, $t_{\max}$ is the time of occurrence of the maximum demand, V_B is the nominal battery voltage, η_B is the battery energy efficiency and $P_L(t)$ is the load demand at time, t. T can be obtained by solving (12) iteratively and can be used in (9) and (10) to obtain SDR and DR_{Sat}. Normally, the time of occurrence of the peak load and the length of evening load period would not be significantly different between two consecutive days. Therefore, once the system is installed and commissioned using the initial historical load curve, the information on t_1 and t_2 can be updated daily from measurements at the PCC to accurately estimate the intended period of discharge.

The flow chart of the charge and discharge control system for a given time step is shown in Fig. 9(a) and 9(b), respectively.
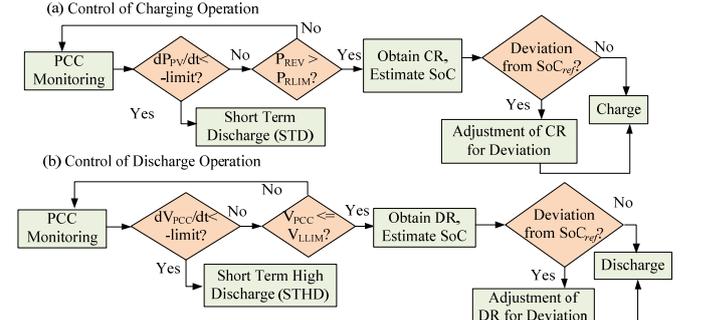

Fig. 9. Storage control flow charts. (a) charging operation (b) discharging operation

The storage device is normally charged if there is no sudden decrease in PV output at the PCC and also a reverse power flow greater than a threshold level is found. The charging rate is obtained using (8) based on the parameters obtained from (9)-(10). The storage is normally discharged if the PCC voltage is found to be lower than a threshold level and also when no sudden dip in the PCC voltage is observed, as shown Fig. 9(b). The discharge rate is obtained using (11) based on the parameters obtained from (9)-(10).

The PV output may be suddenly decreased by irregularities in the sun irradiance levels due to unstable weather conditions causing fluctuations in the PCC net power and voltage. In the event of a sudden decrease in the PV output, the storage is put into a short-term discharge (STD) mode, as shown in Fig. 9(a). The short-term discharge-support is limited to avoid a significant drainage of charge.
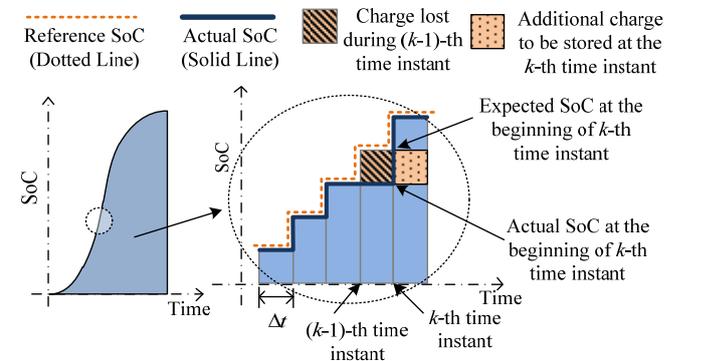

Fig. 10. Adjustment of charging rate to make-up for charge lost due to unstable weather condition.

To ensure an effective use of the available storage capacity, it is necessary to make-up for the charge lost during the short-term discharge period, and also during the unavailability of

enough surplus power at the PCC caused by changing cloudiness of the sky. The lost charge can be replenished by adjusting the charging rate at each instant of time to attain a reference SoC level. The reference SoC level is the one which is not affected by any unstable weather condition and can be obtained using the charging rate expressions given in (8). The strategy for performing the adjustment in charging rate is shown in Fig. 10.

If the storage is not charged at the $(k-1)$-th time instant, the SoC will remain at the same value as in the previous time instant. Again, if the storage is discharged at the $(k-1)$-th time instant, the SoC level will be reduced than the previous SoC. Therefore, an adjustment of the charging rate has to be performed at the beginning of the k-th time instant to make-up for the charge not stored, or lost, during the $(k-1)$-th instant, as given below.

$$CR'(k) = CR(k) + \varepsilon \times \frac{SoC_{ref}(k) - [SoC(k-1) + CR(k) \times \Delta t]}{\Delta t} \quad (13)$$

where, $CR'(k)$ is the adjusted charging rate, SoC_{ref} is the reference level of SoC, Δt is the time between two consecutive time instants, and ε is a parameter defining the percentage of the deviation to be met which can be controlled to limit the adjustment in the charging rate, if required. This adjustment of charging rate ensures an effective utilization of a storage device compared to a constant charging rate strategy in the event of irregularities in PV output which is difficult to anticipate.

Similarly, in the evening, it may be required to discharge the storage at a rate higher than the normal rate to support any abrupt voltage drop, such as a voltage-dip event caused by a sudden increase in the load demand. In this situation, the storage is put into at a short-term high discharge (STHD) mode as presented in Fig. 9(b), depending on the intensity of the sudden increase in the momentary load demand. This will result an additional charge to be drained during the higher discharge operation. Therefore, the discharge rate is adjusted by using (14) to reduce the deviation with the reference SoC level.

$$DR'(k) = DR(k) - \varepsilon \times \frac{SoC_{ref}(k) - [SoC(k-1) - DR(k) \times \Delta t]}{\Delta t} \quad (14)$$

All of the distributed storage units in the feeder operate according to the control strategy described above, based on the local information at the PCC, such as the PV output, the local demand, and the PCC voltage.

Although this paper proposes a storage control strategy based on local parameters only, a coordinated control strategy of multiple storage devices in the feeder may also be possible if a communication system become available as envisaged in the future smart grid. In such a coordinated operation, the storage devices at different locations would be able to exchange information on the available storage capacity and the surplus power at different PCCs using the communication systems, to make a better use of the total storage capacity available in the feeder to store an optimum amount of total excess PV generation in the feeder.

The present paper mainly discusses the mitigation of reverse power flow caused by active power injection from rooftop solar PV in LV distribution feeders, resulting in the avoidance of a voltage-rise, although the system does not intentionally control the voltage. As there is no voltage control set-point in the proposed strategy, it is different than an on load tap-changer or voltage regulator located in medium voltage system where a feed-back arrangement is used to control the voltage at the load centre. For the same reason, it will not interfere with the operation of the on load tap-changer or the voltage regulator. The only effect of this controller is to make the on-load tap changer and the voltage regulator to have less switching operation and hence less stress. With a communication system, the battery storage system can be coordinated with the on-load tap changer as presented in [9].

IV. CASE STUDIES

A distribution network containing medium and low voltage feeders has been extracted from a New South Wales Distribution system in Australia to investigate the applicability of the proposed mitigation strategy. This is an 80 km long 11 kV rural network with three series voltage regulators. A single line diagram of the network is shown in Fig. 11. One of the LV feeders is shown in detail in a dashed circular shape. The LV feeder data used for analysis are presented in Table I.
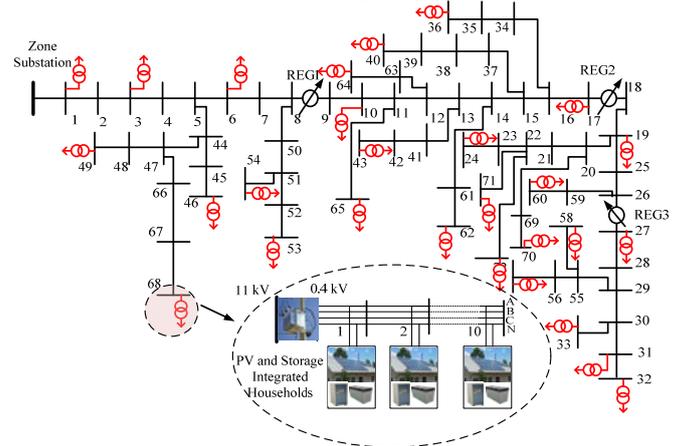

Fig. 11. A practical distribution system in Australia.

TABLE I
DATA OF A TYPICAL AUSTRALIAN LOW VOLTAGE FEEDER

Feeder Length (metre)	350
Pole to Pole Distance (metre)	30-40
Conductor	7/3.00 AAC
MV/LV Transformer Size	160 kVA
PV Size (kW)	2-4 kW
PV Module Manufacturer	Kyocera
Inverter Manufacturer	SMA Sunnyboy
Battery Storage Model	Lead-acid Trojan L-16W
Battery Storage Voltage (V)	2×12
Battery Storage Capacity (Ah)	250

Typical electric appliances used in residential households were used to model the aggregate loads at the different phases of the test feeder. The PV system sizes at the residential households were limited within 4 kW range and operated at unity power factor. The selection of a proper sizing methodology for energy storage is a complex task and may

require optimization process, as discussed in [19], and therefore it is beyond the scope of this paper. In this research, a lead-acid energy storage device rated at 250 Ah, 24 V, was integrated at each of the rooftop PV system which is a typical size for residential rooftop PV applications in Australia for a PV rating of 2-4 kW [20]. The standard charging/discharging curves of a 12-V lead-acid battery available in [13] were used to model a 24-V lead-acid battery using the method described in Section III-A and the obtained charging/discharging curves are shown in Fig. 12. The specifications of the charging/discharging control strategy are given in Table II. The charging/discharging parameters CR_{Sat}, DR_{Sat}, SCR, and SDR are calculated using (9)-(10).

The network analysis is performed using a three-phase four-wire power-flow tool [21] developed by the authors, based on the current mismatch variant of the Newton-Raphson power flow algorithm [22]. The proposed storage control strategy is tested with steady-state simulations of the test network at each instant of time under consideration.
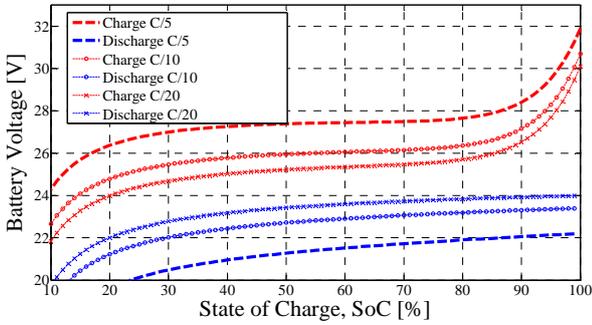

Fig. 12. Charge/discharge curves of a 24-V lead acid battery modeled for different charging/discharging rates.

TABLE II
SPECIFICATIONS OF CHARGING/DISCHARGING CONTROL STRATEGY

Parameter	Value
CR_{Sat}, DR_{Sat}	C/6.56, C/3.34
SCR, SDR (per minute)	0.1619, 0.6243
Charging and Discharging Profile	Triangular
ToS_1, ToS_2	70%, 70%
SoC_{max}, DoD_{max}	100%, 40%
ε for CR, DR compensation	100%

To test the developed methodology in a realistic PV generation environment, a solar PV output profile captured on the 9th of February 2011, in the Renewable Energy Integration Facility, CSIRO Energy Technology, Australia, is used. The PV output, the load demand, the energy storage power and the net active power injection into the grid from 8:00 hours to 24:00 hours for the PCC corresponding to phase *a* of node 10 of the test LV feeder is shown in Fig. 13(a). The PV output was distorted by the sudden changes in the sun irradiance level. It is assumed that the SoC of the storage device is at DoD_{max} at the start of the simulation.

The storage starts to charge at about 9:00 hours by detecting a reverse power flow larger than a set threshold of 0.1 kW at the PCC. Using a triangular charging profile, the charging rate increases at the SCR specified in Table II until it attains ToS_1, which is 70% of the total battery capacity. The SoC profile is shown in Fig. 13(b). Due to the triangular charging profile, the second threshold ToS_2 is also 70%, and

therefore, the charging rate starts to decrease from this point at the same SCR until the charging rate becomes *zero*. Due to the power consumed by the storage in the charging operation, the active power injection into the grid without storage (dotted blue line) in Fig. 13(a) is higher than the active power injection with storage (solid blue line).

Within the charging period, several fluctuations in PV output appear, as marked using the dotted circular shapes in Fig. 13(a). The proposed control strategy detects the sudden changes in PV output and places the storage in a short-term discharge mode, as observed by the negative spikes in the battery power shown in Fig. 13(a). This counteracts the sudden fluctuations in the PV power. As a result, the fluctuations in surplus power injection at the PCC are also reduced, as observed by comparing the solid and dotted blue lines in Fig. 13(a). The drops in the SoC levels in the zoomed box in Fig. 13(b) indicate the short-term discharges. It is also observed in Fig. 13(b) that the SoC level without the charging rate adjustment does not reach the SoC_{max} level.
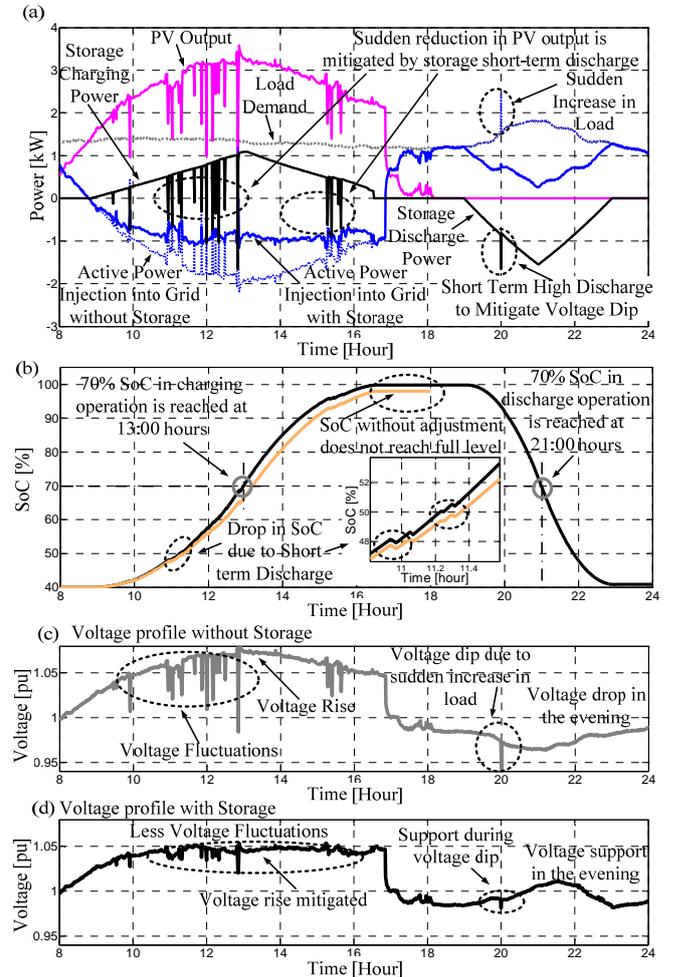

Fig. 13. (a) Load demand, PV output, storage power and active power injection into grid; (b) SoC profile; (c) Voltage profile without storage; (d) Voltage profile with storage.

The discharge operation starts at 19:00 hours by detecting the drop of PCC voltage below a threshold level. Using a triangular discharge profile, the discharge rate increases at the SDR defined in Table II until the SoC drops to 70% of the

SoC and then decreases at the same SDR until DoD_{max} is reached. The discharge power of storage and the SoC during the discharge operation is shown in Fig. 13(a) and 13(b), respectively. A sudden increase in the PCC load (due to an event such as a motor start) is observed in Fig. 13(a) at about 20:00 hours. This is partly mitigated by putting the storage in a short-term high discharge mode, as observed in Fig. 13(a) by a momentary increase in storage discharge power.

The PCC voltage profile with and without storage is shown in Fig. 13(c) and 13(d), respectively. The voltage-rise during the peak PV generation, the voltage fluctuations during the sudden reductions in PV output, the voltage drop during the evening peak and a voltage dip due to a sudden increase in the load are observed in Fig. 13(c). Fig. 13(d) shows that the voltage-rise is reduced by the charging operation; the voltage fluctuations are reduced by the short-term discharging operation; the voltage profile is improved during evening peak by the discharging operation; and the voltage dip is partly mitigated by the short-term high discharge operation.

A comparison of the reverse power flow at the secondary side of LV substation connected at bus 68 in Fig. 11 with and without distributed storage devices is shown in Fig. 14. It is observed that the reverse power flow with storage devices is reduced by 44% compared to the case without storage devices.

The reduction in reverse power flow is limited due to the size of the installed storage devices. With a sufficient storage capacity, it is possible to totally eliminate the reverse power. The only limitation is the cost of the energy storage system. A trade-off analysis between the cost of the energy storage and the impacts of the reverse power flow and voltage-rise in the system has to be performed to find the optimum size of the energy storage system. Further, it is important to note that the reverse flow is a complex function of time, load demand and sun insolation. The result in Fig. 14 is only for a particular day, a particular load demand and the given sun insolation profile. The size of the energy storage system has been found to be adequate for the size of PV modules chosen in terms of the acceptable Australian voltage limits.
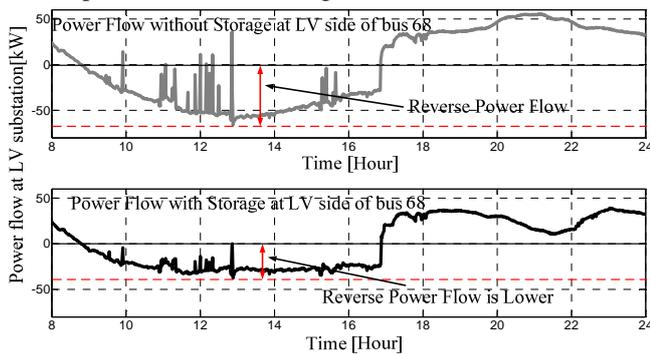

Fig. 14. Reverse power flow mitigation with storage.

A case is studied in Fig. 15 where the PV generation drops down to such a low level for a certain period that no surplus power is available at the PCC for the storage to be charged during that time. The PV output profile is obtained from the same source (Renewable Energy Integration Facility at CSIRO), and the data was captured on the 8th February, 2011. As shown in Fig. 15(a), the PV output drops below the load

demand in the period from 10:00 hours to about 11:30 hours. At this time, no reverse power is available at the PCC and the storage device is not charged. The PV output again exceeds the load demand from about 11:45 hours and the storage device consumes the surplus power available at the PCC. The storage charging follows a triangular profile. The charging rate starts to decrease once 70% SoC level is reached at about 13:30 hours, as shown in Fig. 15(b). It is important to observe that due to multiple short-term discharge operations from 14:00 hours to 16:30 hours, and the unavailability of surplus PV power from 16:30 hours, the desired SoC_{max} level is not reached at the end of the charging period. The SoC level in this scenario reaches to about 88.5%. To ensure that the available stored charge is used wisely to serve the evening peak load, the discharge parameters are re-calculated using (9)-(11). In this case, the discharge rate starts to decrease when the SoC drops to 65.2% (not to 70% that would be the case for full SoC level) at 21:00 hours as shown in Fig 15(b). The mitigation of voltage-rise, the reduction of voltage fluctuations, and voltage support during the evening peak demand are shown in Fig. 15(c) and 15(d).
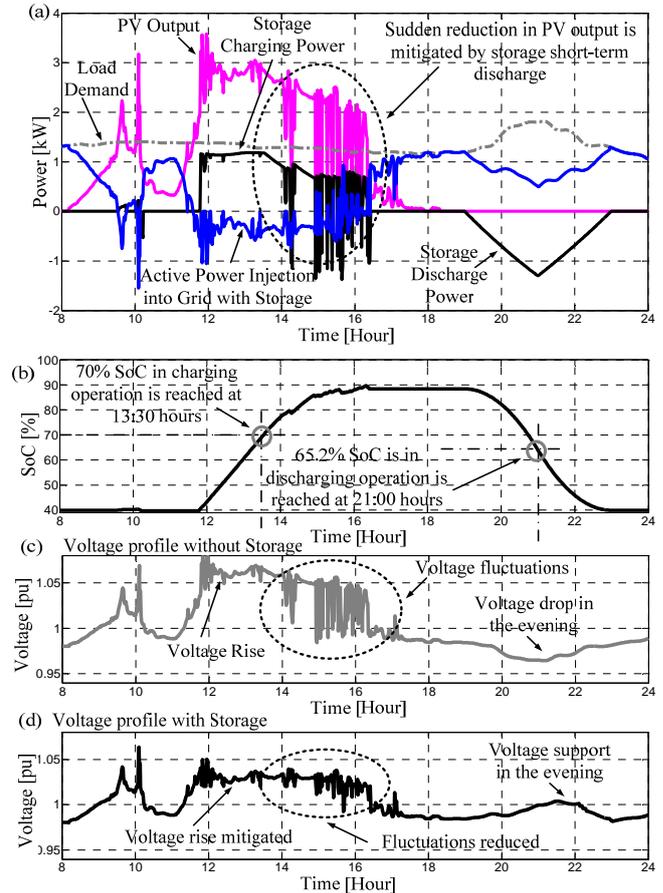

Fig. 15. (a) Load demand, PV output, storage power and active power injection into grid; (b) SoC profile; (c) Voltage profile without storage; (d) Voltage profile with storage.

The usefulness of the proposed charging strategy is shown in Fig. 16 for the same PV output profile in terms of the utilization of battery capacity and the mitigation of voltage-rise. Fig. 16(a) shows that the storage power consumption is higher with the charging rate adjustment than that without the

adjustment, because according to (13), the charging rate is adjusted to be higher than the normal charging rate to recover the charge not stored during the time of unavailability of surplus PV power. Also, the storage power consumption is higher with the proposed strategy than that with the constant charging strategy during peak PV generation period.

Fig. 16(b) shows that at the end of the charging period, 28% higher utilization of the storage capacity is achieved by the proposed adjustment strategy when compared to the constant charging strategy (220Ah instead of 150Ah). However, if the adjustment is not performed to account for unstable weather condition, the utilization of the battery capacity would not be significantly higher than constant charging rate, as shown in Fig. 16(b). Fig. 16(c) shows that the proposed strategy can mitigate voltage-rise better than that using the constant charging rate, particularly during peak PV period in the midday.
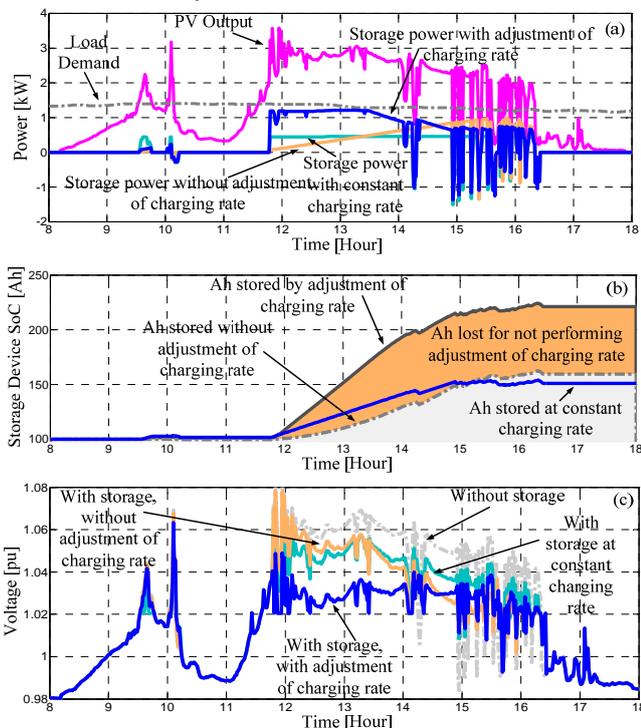

Fig. 16. Usefulness of the proposed charging strategy. (a) effect on power consumed by storage in charging operation; (b) utilization of battery capacity (c) voltage rise mitigation performance.

The methodology proposed in this paper is generic in nature and can be adapted for any integrated PV and storage system connected to the PCC. It can be used by the distribution network operators as a general guideline for the charging/discharging of storage devices integrated at the LV customer premises with rooftop PV. Further, a graphical user interface can be developed to allow network operators to input the relevant information such as the intended length of charging/discharging period and the shape of the charging/discharging profile, the PV irradiance data, the PV rating, the PV inverter characteristics, the energy storage data, such as rating, charging/discharging characteristics, SoC_{max}, DoD_{max}. It is envisaged that with the availability of smart meters and monitoring devices, especially with the

introduction of Advanced Metering Infrastructure [23], the low voltage distribution networks will be automated using a two-way communication with the utility system. Through this arrangement, the AMI interface can communicate with network control center and the required parameters for storage controller can be made available. In such an environment, the distributed storage devices will be able to mitigate the PV impacts using the continuously updated control parameters. A manual can be developed and used to inform the operators on how to input the correct data to the graphical user interface to obtain a generic charging/discharging strategy for an integrated PV and storage system under consideration.

V. Conclusion

A new strategy for charging/discharging of storage devices has been proposed in this paper for rooftop PV impact mitigation and evening peak load support. The proposed strategy can match the PV output/evening load profile better than the traditional constant charging/discharging strategy. A methodology has been developed to obtain the appropriate charging/discharging rates based on the current SoC level of the storage device and the intended charging/discharging period to wisely utilize the limited capacity of storage device. Further, the proposed strategy can mitigate sudden changes in PV output due to unstable weather conditions by putting the storage in a short-term discharge operation mode. It can also track and compensate for the deviation of the storage SoC from the desired level of SoC. Simulation results demonstrate that the proposed mitigation strategy can effectively mitigate the negative impacts of solar PV, can support the evening peak-time load demand while utilizing the available capacity of the storage device.

VI. Acknowledgment

VII. References

[1] A. Canova, L. Giaccone, F. Spertino, and M. Tartaglia, "Electrical Impact of Photovoltaic Plant in Distributed Network," *IEEE Transactions on Industry Applications* vol. 45, pp. 341-347, 2009.

[2] M. Thomson and D. G. Infield, "Network Power-Flow Analysis for a High Penetration of Distributed Generation," *IEEE Transactions on Power Systems* vol. 22, pp. 1157-1162, 2007.

[3] R. Tonkoski, D. Turcotte, and T. H. M. El-Fouly, "Impact of High PV Penetration on Voltage Profiles in Residential Neighborhoods," *IEEE Transactions on Sustainable Energy,* vol. 3, pp. 518-527, 2012.

[4] R. A. Walling, R. Saint, R. C. Dugan, J. Burke, and L. A. Kojovic, "Summary of Distributed Resources Impact on Power Delivery Systems," *IEEE Transactions on Power Delivery* vol. 23, pp. 1636-1644, 2008.

[5] R. Tonkoski, L. A. C. Lopes, and T. H. M. El-Fouly, "Coordinated Active Power Curtailment of Grid Connected PV Inverters for Overvoltage Prevention," *IEEE Transactions on Sustainable Energy,* vol. 2, pp. 139-147, 2011.

[6] E. Demirok, P. González, K. H. B. Frederiksen, D. Sera, P. Rodriguez, and R. Teodorescu, "Local Reactive Power Control Methods for Overvoltage Prevention of Distributed Solar Inverters in Low-Voltage Grids," *IEEE Journal of Photovoltaics* vol. 1, pp. 174-182, 2011.

[7] Y. Liu, J. Bebic, B. Kroposki, J. de Bedout, and W. Ren, "Distribution System Voltage Performance Analysis for High-Penetration PV," in *IEEE Energy 2030 Conference*, Atlanta, GA, USA, 17-18 Nov., 2008, pp. 1-8.

[8] P. M. S. Carvalho, P. F. Correia, and L. A. F. Ferreira, "Distributed Reactive Power Generation Control for Voltage Rise Mitigation in Distribution Networks," *IEEE Transactions on Power Systems* vol. 23, pp. 766-772, 2008.

[9] L. Xiaohu, A. Aichhorn, L. Liming, and L. Hui, "Coordinated Control of Distributed Energy Storage System With Tap Changer Transformers for Voltage Rise Mitigation Under High Photovoltaic Penetration," *IEEE Transactions on Smart Grid,* vol. 3, pp. 897-906, 2012.

[10] Y. Ueda, K. Kurokawa, T. Tanabe, K. Kitamura, K. Akanuma, M. Yokota, and H. Sugihara, "Study on the Over Voltage Problem and Battery Operation for Grid-connected Residential PV Systems," in *22nd European Photovoltaic Solar Energy Conference*, Milan, Italy, 2007.

[11] M. J. E. Alam, K. Muttaqi, and D. Sutanto, "Distributed Energy Storage for Mitigation of Voltage-rise Impact caused by Rooftop Solar PV," in *IEEE PES General Meeting*, San Diego, California, USA, 22-26 July, 2012.

[12] I. Papic, "Simulation Model for Discharging a Lead-acid Battery Energy Storage System for Load Leveling," *Energy Conversion, IEEE Transactions on,* vol. 21, pp. 608-615, 2006.

[13] R. Perez, "Lead-acid Battery State of Charge vs. Voltage," *Home Power,* vol. 36, pp. 66-69, 1993.

[14] G. M. Masters, *Renewable and Efficient Electric Power Systems*. New Jersey: Wiley-IEEE Press, 2004.

[15] N. K. Medora and A. Kusko, "Dynamic Battery Modeling of Lead-Acid Batteries using Manufacturers' Data," in *Twenty-Seventh International Telecommunications Conference,* Berlin, Germany, Sept. 2005, pp. 227-232.

[16] O. Tremblay, L. A. Dessaint, and A. I. Dekkiche, "A Generic Battery Model for the Dynamic Simulation of Hybrid Electric Vehicles," in *Vehicle Power and Propulsion Conference,* Arlington, TX, USA, 9-12 Sept., 2007, pp. 284-289.

[17] R. Rynkiewicz, "Discharge and Charge Modeling of Lead Acid Batteries," in *Fourteenth Annual Applied Power Electronics Conference and Exposition*, Dallas, TX, USA, 14-18 Mar, 1999, pp. 707-710 vol.2.

[18] D. Linden and T. B. Reddy, "Handbook of Batteries," *New York,* 1995.

[19] Y. Ru, J. Kleissl, and S. Martinez, "Storage Size Determination for Grid-Connected Photovoltaic Systems," *accepted for a future issue of IEEE Transactions on Sustainable Energy* 2012.

[20] K. Y. Khouzam, "Technical and Economic Assessment of Utility Interactive PV Systems for Domestic Applications in South East Queensland," *IEEE Transactions on Energy Conversion,* vol. 14, pp. 1544-1550, 1999.

[21] M. J. E. Alam, K. M. Muttaqi, and D. Sutanto, "A Three-Phase Power Flow Approach for Integrated 3-Wire MV and 4-Wire Multigrounded LV Networks with Rooftop Solar PV," *Accepted for a future issue of IEEE Transactions on Power Systems*.

[22] D. R. R. Penido, L. R. de Araujo, S. Carneiro, J. L. R. Pereira, and P. A. N. Garcia, "Three-Phase Power Flow Based on Four-Conductor Current Injection Method for Unbalanced Distribution Networks," *IEEE Transactions on Power Systems* vol. 23, pp. 494-503, 2008.

[23] R. C. Dugan and M. McGranaghan, "Sim City," *Power and Energy Magazine, IEEE,* vol. 9, pp. 74-81, 2011.

BIOGRAPHIES

M J E Alam (Std. Member'10) received B.Sc. and M.Sc. Degree in Electrical and Electronic Engineering from Bangladesh University of Engineering and Technology, Dhaka, Bangladesh, in 2005 and 2009, respectively, with focus on electrical energy and power systems.

At present he is working towards PhD degree at the University of Wollongong, New South Wales, Australia. His research interest includes modeling and analysis of power systems considering the impacts of distributed and renewable energy resources.

Prior to starting PhD studies, he has been involved with the power industry in Bangladesh for 4.5 years, where he worked in the field of power generation, transmission and distribution.

K M Muttaqi (M'01, SM'05) received the Ph.D. degree from Multimedia University, Malaysia, in 2001. Currently, he is an Associate Professor at the School of Electrical, Computer, and Telecommunications Engineering, University of Wollongong, Wollongong, Australia. He is an Associate Editor of IEEE Transactions on Industry Applications. He was associated with the University of Tasmania, Australia as a Research Fellow/Lecturer/Senior Lecturer from 2002 to 2007, and with the Queensland University of Technology, Australia as a Research Fellow from 2000 to 2002. Previously, he also worked for Multimedia University as a Lecturer for three years. His special fields of interests include distributed generation, renewable energy, power system planning, intelligent grid, and power system reliability.

D Sutanto (SM'89) obtained his BEng. (Hons) and PhD from the University of Western Australia. He is presently the Professor of Power Engineering at the University of Wollongong, Australia. His research interests include power system planning, analysis and harmonics, FACTS and Battery Energy Storage systems. He is a Senior Member of IEEE. He is currently the IEEE IAS Area Chair for Region 10 (Asia Pacific).